Visualization of Chiral Electronic Structure and Anomalous Optical Response in a Material with Chiral Charge Density Waves

H. F. Yang,[1,*] K. Y. He,[2,*] J. Koo,[3,*] S. W. Shen,[1] S. H. Zhang,[1] G. Liu,[2] Y. Z. Liu,[3] C. Chen,[1,4] A. J. Liang,[1,5] K. Huang,[1] M. X. Wang,[1,5] J. J. Gao,[6] X. Luo,[6] L. X. Yang,[7] J. P. Liu,[1,5] Y. P. Sun,[6,8,9] S. C. Yan,[1,5] B. H. Yan,[3,†] Y. L. Chen,[1,4,5,7,‡] X. Xi,[2,9,§] and Z. K. Liu[1,5,‖]

[1]*School of Physical Science and Technology, ShanghaiTech University, Shanghai 201210, People's Republic of China*
[2]*National Laboratory of Solid State Microstructures and Department of Physics, Nanjing University, Nanjing 210093, People's Republic of China*
[3]*Department of Condensed Matter Physics, Weizmann Institute of Science, Rehovot 76100, Israel*
[4]*Department of Physics, University of Oxford, Oxford, OX1 3PU, United Kingdom*
[5]*ShanghaiTech Laboratory for Topological Physics, Shanghai 201210, People's Republic of China*
[6]*Key Laboratory of Materials Physics, Institute of Solid State Physics, Chinese Academy of Sciences, HFIPS, Hefei 230031, People's Republic of China*
[7]*State Key Laboratory of Low Dimensional Quantum Physics and Department of Physics, Tsinghua University, Beijing 100084, People's Republic of China*
[8]*High Magnetic Field Laboratory, Chinese Academy of Sciences, HFIPS, Hefei, 230031, People's Republic of China*
[9]*Collaborative Innovation Center of Advanced Microstructures, Nanjing University, Nanjing 210093, People's Republic of China*

(Received 16 May 2022; accepted 7 September 2022; published 7 October 2022)

Chiral materials have attracted significant research interests as they exhibit intriguing physical properties, such as chiral optical response, spin-momentum locking, and chiral induced spin selectivity. Recently, layered transition metal dichalcogenide $1T$-TaS_2 has been found to host a chiral charge density wave (CDW) order. Nevertheless, the physical consequences of the chiral order, for example, in electronic structures and the optical properties, are yet to be explored. Here, we report the spectroscopic visualization of an emergent chiral electronic band structure in the CDW phase, characterized by windmill-shaped Fermi surfaces. We uncover a remarkable chirality-dependent circularly polarized Raman response due to the salient in-plane chiral symmetry of CDW, although the ordinary circular dichroism vanishes. Chiral Fermi surfaces and anomalous Raman responses coincide with the CDW transition, proving their lattice origin. Our Letter paves a path to manipulate the chiral electronic and optical properties in two-dimensional materials and explore applications in polarization optics and spintronics.

DOI: 10.1103/PhysRevLett.129.156401

Chiral objects are ubiquitous in nature, from gigantic galaxy to microscopic DNA structure [1–3]. They host fundamental physics (such as parity violation of subatomic weak interaction) and are essential for life (homochirality of natural biomolecules) [1–3]. In condensed-matter systems, materials with chiral electronic states exhibit intriguing optical, magnetic, and transport properties and have attracted great research interest [1,2,4–7]. In principle, crystals with a chiral lattice structure naturally exhibit chiral electronic band structures. One example is the chiral topological semimetals, whose chiral crystal symmetry enforces chiral surface Fermi arcs that are expected to display numerous exotic physical phenomena such as circular dichroism, unusual photogalvanic effect, and nonreciprocal transport [4,8–11].

The chiral electronic structure can emerge alternatively in materials with achiral crystal structure. Because of the limited material choice, such emergent chiral electronic structure and its unique physical properties has not been investigated. The layered transition metal dichalcogenide $1T$-TaS_2 provides such an opportunity. It hosts an achiral crystal structure with both inversion and mirror symmetries preserved in its high-temperature normal state [Fig. 1(a)]. Upon cooling down, $1T$-TaS_2 transits to an incommensurate CDW (ICDW) phase at around 550 K, nearly commensurate CDW (NC-CDW) phase at around 350 K, and finally commensurate CDW (CCDW) phase at 180 K [12–14]. The CCDW phase features commensurate lock-in of star-of-David clusters under $\sqrt{13} \times \sqrt{13}$ reconstruction [Fig. 1(b)], in which the reconstructed superlattice rotates by 13.9° with respect to the pristine lattice [Figs. 2(c) and 2(d)], thus breaking the mirror symmetry while preserving the inversion symmetry, which is addressed as the chiral CDW phase. The chiral CDW state is investigated for intriguing phenomena, such as cluster Mott insulator [15,16], quantum spin liquid [17–19], superconductivity under pressure [20], carrier doping [21–23], and isovalent substitution [24–26]. Because of the existence of inversion symmetry, such a chiral CDW exhibits no circular dichroism which can probe

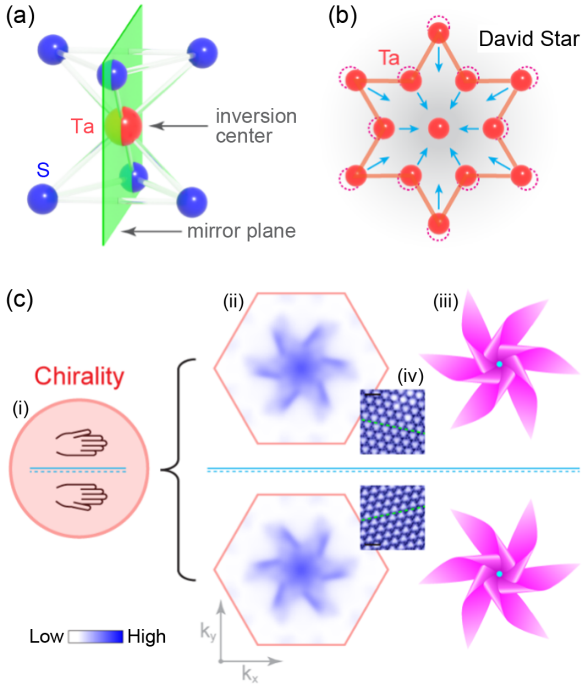

FIG. 1. (a) Schematic of crystal structure of 1T-TaS_2 in the normal state, which is achiral as both inversion and mirror symmetries are preserved. (b) Sketch of the David-Star clusters in the CCDW state. (c) The hidden chiral order in 1T-TaS_2, which is featured by the chiral CDW and windmill-shape band structure with broken mirror symmetry. (i)–(iv) are the sketch of chirality, calculated constant-energy contour at −0.1 eV and related schematic, topography via STM (sample bias: 500 mV, tunneling current: 19 pA, sample temperature: 4.3 K; scale bar 1 nm), respectively.

the conventional chirality. However, the direct physical impacts, e.g., the chiral electronic structure and the consequent optical properties, of the chiral order have not been addressed [25,27–41].

In this Letter, by performing angle-resolved photoemission spectroscopy (ARPES) measurements on 1T-TaS_2 with high quality, we discover a chiral electronic structure emergent in the chiral CDW phase of 1T-TaS_2 [Fig. 1(c)]. The chiral electronic structure appears as windmill shape Fermi contours with two distinct handedness on different samples and domains. Remarkably, although the chiral electronic structure shows no circular dichroism in optical reflectivity, we observe an anomalous, chirality-dependent circularly polarized Raman response, induced by the CDW-induced symmetry breaking. Furthermore, across the CDW phase transition at 350 K, we observe a simultaneous chiral transition in the electronic structure and Raman response, thus proving their common lattice origin as the chiral CDW order. Our Letter reveals a mechanism to generate chiral electronic structures with unique anomalous Raman responses (Supplemental Material [42]). The chiral electronic structures in 1T-TaS_2 host application potentials on polarization optics and spintronics [55–57], nanoelectronics based on mirror domain walls [58], CDW-based memory [58], stereo chemistry and pharmacology [59,60], etc.

Figure 2(a) plots the measured band structure of 1T-TaS_2 in the CCDW phase. From the Fermi energy to high binding energy, the constant energy contours (CECs) clearly demonstrate counterclockwise windmill shape features, as shown by three representative CECs at different binding energies [Figs. 2(a)(i)–2(a)(iii)]. These windmill shaped CECs are nicely reproduced by our *ab initio* calculations [Figs. 2(a)(iv)–2(a)(vi)] (calculation details can be found in Supplemental Material [42], Notes S1 and S3). We rule out the origin of the windmill shape being the photoemission matrix element effect by systematic polarization and photon-energy dependent ARPES measurements (Supplemental Material [42], Note S4 and Fig. S1). As the windmill shape features break the mirror symmetry (they cannot be overlapped with their mirror images), we could describe them as chiral electronic structures [1,60].

Interestingly, the other type of chiral electronic structure rotating clockwise [Fig. 2(b)] could be obtained from another sample (and also from different regions on the same sample, see Supplemental Material [42], Fig. S2). The three representative CECs [Figs. 2(b)(i)–2(b)(iii)] nicely match the mirror images of Fig. 2(a)(i)–2(b)(iii), suggesting they are of the same physical origin only with opposite chirality.

We attribute the origin of the chiral electronic structure to the emergent chiral CCDW state, since 1T-TaS_2 crystallizes in the achiral space group of P-3m1 (No. 164) with both mirror and inversion symmetries [Fig. 1(a)]. The commensurate lock-in of star-of-David clusters leads to the rotation of 13.9° of the CDW vector with respect to the crystal lattice [14] [Fig. 2(c)], which breaks the mirror symmetry and gives rise to the emergence of in-plane chirality. As the rotation can occur clockwise or counterclockwise, two enantiomers [58,61] with mirrored chiral band structures are formed (Fig. 2) with left and right handedness [Figs. 2(c) and 2(d)], thus different geometrical chirality (Supplemental Material [42], Fig. S3). The two enantiomers (left and right handed) and their rotation angles of ±13.9° are directly confirmed by scanning tunneling microscopy [via topography and the corresponding Fourier analysis in Figs. 2(c) and 2(d)] and ARPES studies as reconstructed band structures match its own reconstructed Brillouin zone (Supplemental Material [42], Figs. S16 and S18).

Although circular dichroism has been observed in compounds with chiral crystal and electronic structure [62], it is not observed in the CCDW phase of 1T-TaS_2, due to the preserved inversion symmetry. Instead, one significant new property of the latter is the chirality-dependent Raman response to circularly polarized light. By definition, a two-dimensional (2D) chiral object is not superimposable on its mirror image by in-plane operations unless it is flipped in three-dimensional space. A 2D chiral crystal necessitates nonzero off-diagonal components for

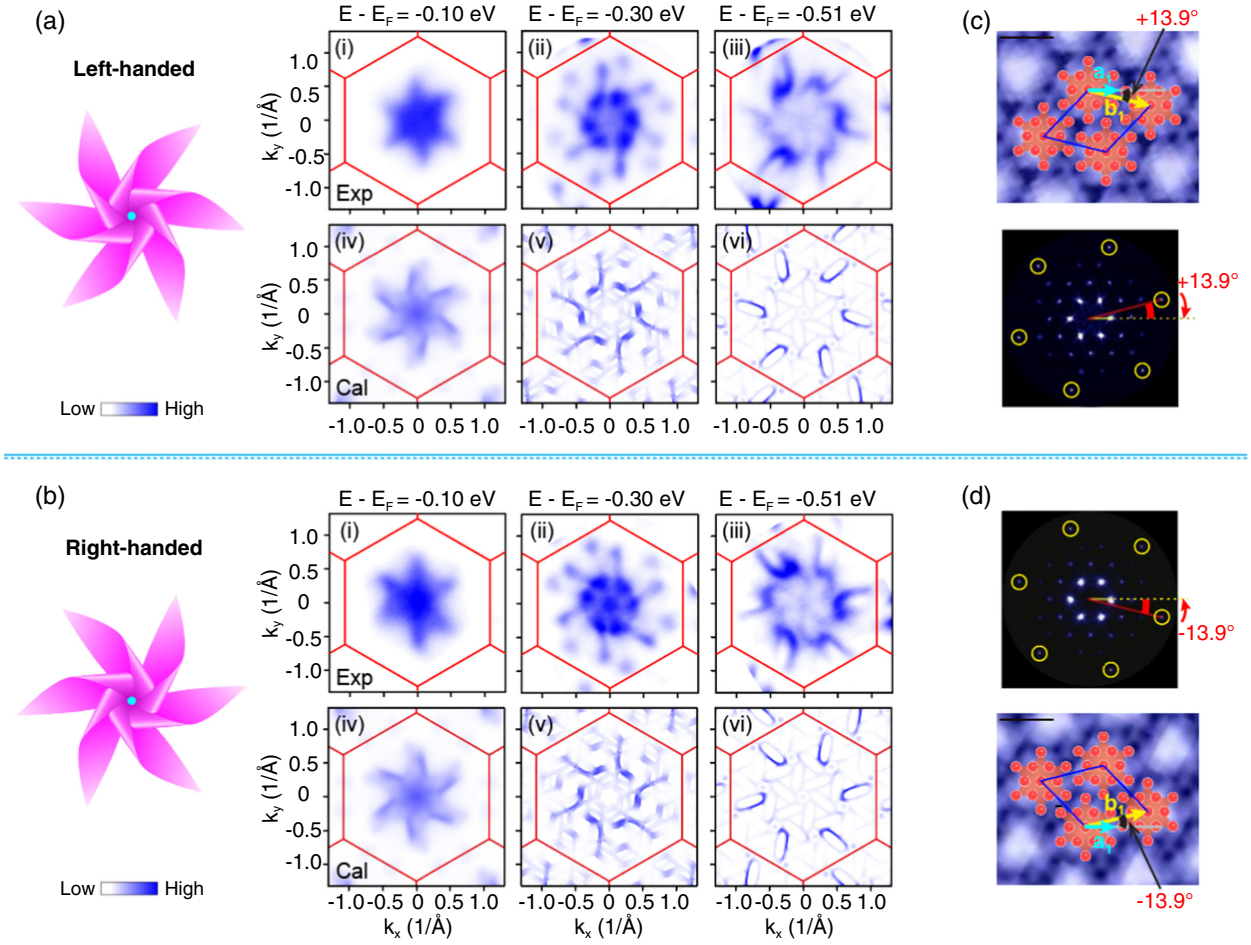

FIG. 2. (a) Windmill-shape band structures of the chiral-left domain of $1T$-TaS_2 in the CCDW phase. (i)–(iii) Representative CECs at −0.1 eV, −0.3 eV, and −0.51 eV measured with 94 eV linearly polarized photons at ∼15 K. (iv)–(vi) Calculated CECs at the corresponding energies. (b) Same as (a) but measured on the chiral-right domain. (c) Topography (upper) and its Fourier transform results (lower) on the chiral-left domain via STM (sample bias: 500 mV, tunneling current: 19 pA, sample temperature: 4.3 K). Scale bar 1 nm. The unit vector of the CCDW (yellow arrow) rotates clockwise by 13.9° with respect to the lattice vector (cyan arrow). Here we show the close-up topography image for better presentation of the rotated supercell, and the raw data are shown in Supplemental Material [42], Fig. S34. (d) Same as (c) but measured on the chiral-right domain. The unit vector of the CCDW (yellow arrow) rotates counterclockwise by 13.9° with respect to the lattice vector (cyan arrow). Discussions on the chiral domain size are presented in Supplemental Material [42], Note S8.

its Raman tensor $\mathbf{R} = \left(\begin{smallmatrix} a & c \\ c & b \end{smallmatrix}\right)$, because the mirror operation on $\mathbf{R}$ yields $\mathbf{R}' = \left(\begin{smallmatrix} a & -c \\ -c & b \end{smallmatrix}\right)$, and nonzero c guarantees $\mathbf{R}' \neq \mathbf{R}$, that is, two chiral counterparts. When the tensor elements are complex, the Raman intensities exhibit a contrast in the circular contrarotating configurations, $I_{\sigma^+\sigma^-} \neq I_{\sigma^-\sigma^+}$, where $\sigma^i\sigma^s(i, s = +, -)$ represents the helicities for the incident and scattered photons [see the measurement schematic in Fig. 3(a)]. More importantly, the two types of chiral structures are distinguishable by the reversed contrast, because $I_{\sigma^+\sigma^-} = I'_{\sigma^-\sigma^+}$ and $I_{\sigma^-\sigma^+} = I'_{\sigma^+\sigma^-}$, where I and I' represent the Raman intensities measured for opposite chiral structures. More detailed discussions can be found in Supplemental Material [42], Note S6.

This type of Raman response is realized in $1T$-TaS_2 in the CCDW phase, because its point group C_{3i} features E_g phonon modes with Raman tensors in the above form [63–65], and its absorbing nature at the excitation photon energy [66] makes the Raman tensors complex. Its Raman spectra show a large number of A_g and E_g phonon modes associated with the CDW superlattice [63–65] [Fig. 3(b)], consistent with our *ab initio* calculations on the star-of-David structure (Supplemental Material [42], Fig. S4). The A_g modes are only detected in the two equivalent circular corotating configurations ($I_{\sigma^+\sigma^+} = I_{\sigma^-\sigma^-}$), whereas the E_g modes exhibit $I_{\sigma^+\sigma^-} \neq I_{\sigma^-\sigma^+}$ as expected. Only the E_g modes can reflect the chirality because they correspond to two degenerate vibrations with clockwise or counterclockwise circling motions of atoms, i.e., two chiral phonon modes with opposite angular momentum (Supplemental Material [42], Fig. S5).

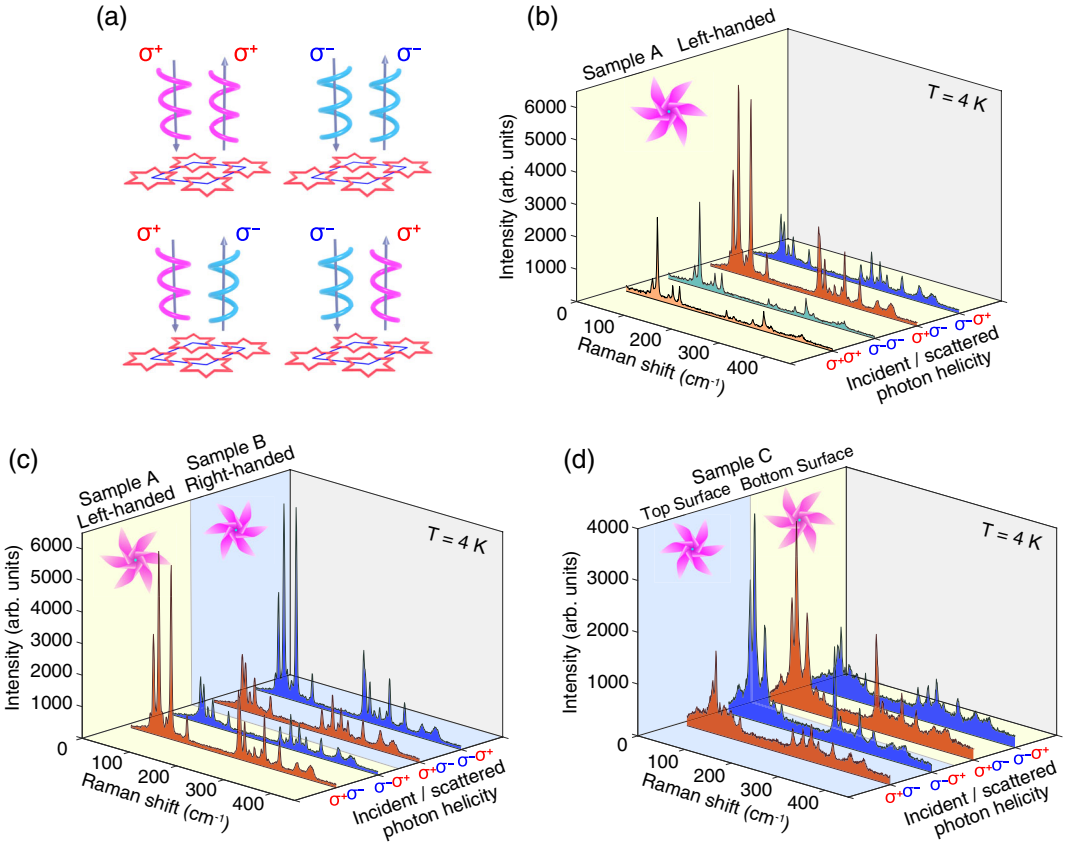

FIG. 3. Photon-helicity-dependent Raman response in CCDW phases of 1T-TaS_2. (a) Schematic of polarization-resolved Raman response measurements. (b) Raman spectra of sample A measured in the circular corotating ($\sigma^+\sigma^+$ and $\sigma^-\sigma^-$) and circular contrarotating ($\sigma^+\sigma^-$ and $\sigma^-\sigma^+$) polarization configurations. (c) Raman spectra of samples A and B showing opposite $\sigma^+\sigma^-/\sigma^-\sigma^+$ response. (d) Swapped $\sigma^+\sigma^-/\sigma^-\sigma^+$ Raman response on the opposite sides of sample C. All Raman spectra taken at $T = 4$ K.

Focusing on the E_g modes in the CCDW phase, the contrasting Raman response $I_{\sigma^+\sigma^-} \neq I_{\sigma^-\sigma^+}$ was reproduced in multiple samples, divided into two groups with opposite chirality (Supplemental Material [42], Fig. S6). Each of them shows homogenous properties. Figure 3(c) shows the Raman spectra of Samples A and B with opposite chirality at 4 K, which are almost identical for exchanged σ^i and σ^s. They are indistinguishable if measured in the linear or circular corotating polarization configurations (Supplemental Material [42], Fig. S7). As a more direct test of the chirality, the spectra taken on the two faces of Sample C agree perfectly when σ^i and σ^s are swapped [see Fig. 3(d) and more details in Supplemental Material [42], Fig. S8]. These results establish a correspondence between the two types of photon helicity-dependent Raman scattering and distinct crystal structures with opposite chirality.

We further investigate the CDW origin of the chirality in the electronic structure and photon-helicity-dependent Raman signal by temperature-dependent ARPES and Raman scattering (Fig. 4). When raising the sample temperature to 370 K (in ICDW) and across the NC-CDW to ICDW transition, the observed band structure becomes quite simple [Fig. 4(a), Supplemental Material [42], Figs. S17 and S25] compared to that of the CCDW state measured at 21 K [Fig. 4(b)]. Specifically, the observed CECs do not show chiral structure anymore and mirror symmetry is restored [one mirror plane is marked by dotted magenta line in Fig. 4(a)(ii)]. This indicates a chiral-to-achiral transition since the rotation angle between the CDW lattice and crystal lattice relaxes to 0° and the mirror symmetry restores via changing temperature, accompanying the disappearing with the geometrical chirality (Supplemental Material [42], Fig. S3). (Empirical tight-binding modellings and discussions on the chiral domain size can be found in Supplemental Material [42], Notes S7 and S8). We note that chiral electronic structure also exists in the NC-CDW phase (between CCDW and ICDW) featuring a rotation of ~12° [14], though the windmill shape is not as evident as that of the CCDW (Supplemental Material [42], Figs. S17 and S28). The disappearing of the chirality also manifests in the temperature-dependent Raman scattering data. Figure 4(d) shows that when temperature is raised from 349 to 355 K across the transition from the NC-CDW to the ICDW

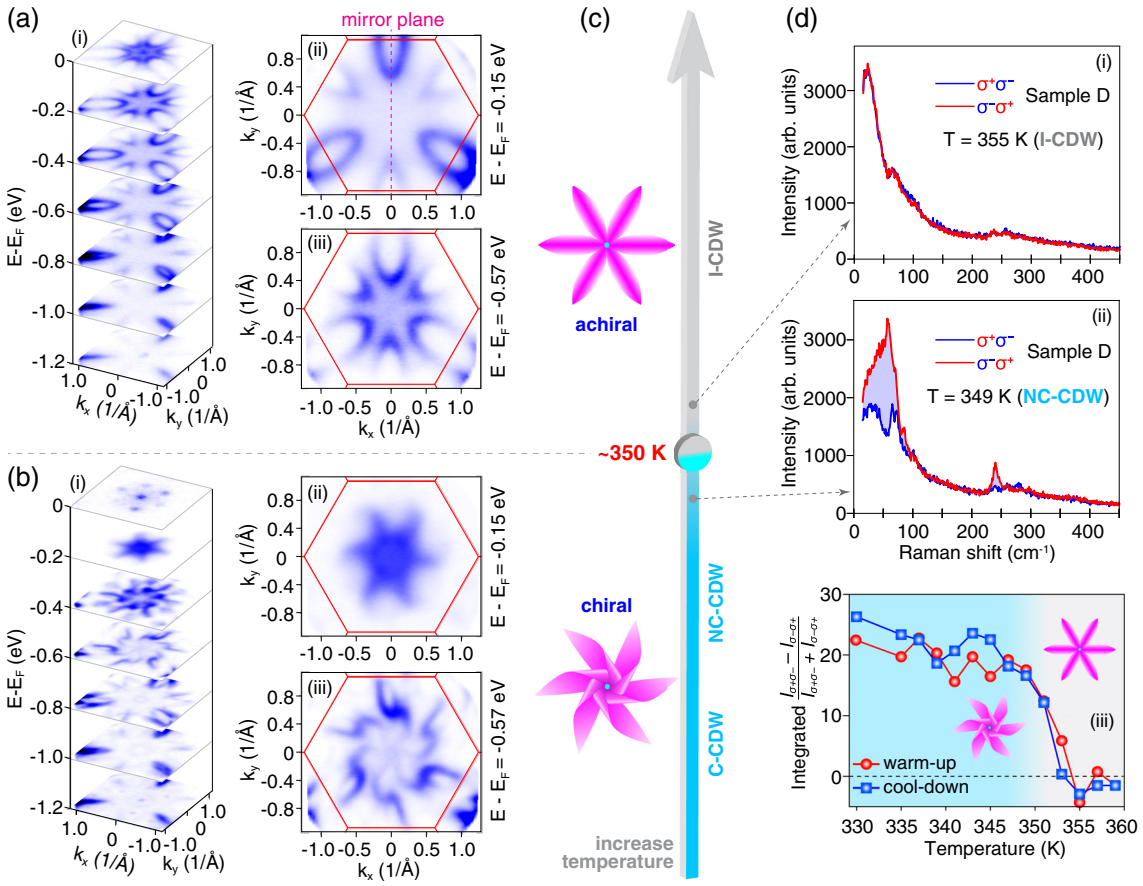

FIG. 4. Chiral-to-achiral transition when elevating temperature to cross ~350 K. (a),(b) Comparison of band structures of 1T-TaS_2 at 21 K (CCDW) (a) and 370 K (ICDW) (b). (c) Schematic illustration of chiral-to-achiral transition at ~350 K. (d) Circular contrarotating Raman response of sample D at 349 K (i) and 355 K (ii). The shaded area in (ii) highlights $I_{\sigma^+\sigma^-} - I_{\sigma^-\sigma^+}$ at 349 K. (iii) Temperature dependence of the normalized differential spectra $(I_{\sigma^+\sigma^-} - I_{\sigma^-\sigma^+})/(I_{\sigma^+\sigma^-} + I_{\sigma^-\sigma^+})$ integrated over 20–300 cm^{-1}, clearly showing the chiral-to-achiral transition occurs ~350 K.

phase, the contrast between the $\sigma^+\sigma^-$ and $\sigma^-\sigma^+$ spectra disappears. This is because the ICDW phase features E_g Raman tensors with only diagonal or off-diagonal components, but not both (see Supplemental Material [42], Note S6). We plot the temperature dependence of the integrated intensity of the normalized differential spectra $(I_{\sigma^+\sigma^-} - I_{\sigma^-\sigma^+})/(I_{\sigma^+\sigma^-} + I_{\sigma^-\sigma^+})$ over $20 - 300$ cm^{-1} [Fig. 4(d)(iii)] which clearly demonstrates the correlation between the chiral Raman response and the chiral CDW phase. The reversibility exhibited in the warming and cooling processes demonstrates efficient control of the electronic chirality as well as Raman responses by temperature. The simultaneous chiral transition in the electronic structure and Raman response thus proves their common lattice origin as the chiral CDW order.

Our observation of chiral Raman spectra points to a new type of optical response from chiral crystal structures. We derive a complete list of point groups with this form of Raman tensor (Supplemental Material [42], Table S1), providing a guide to search for 2D chiral crystals. The uniqueness of the chirality in 1T-TaS_2 lies in its CDW origin, which makes it susceptible to a variety of tuning parameters, such as temperature [12–14], pressure [20], and doping [21–23]. We note that Raman optical activity [67], which measures the difference in the Raman intensity for either incident or scattered σ^+ and σ^- polarized light from chiral molecules, peptides and proteins (chiral structures in 3D), is several orders of magnitude weaker [68].

In summary, we have discovered chiral electronic structure for both enantiomers in 1T-TaS_2 in the CCDW phase. We further show that the chirality naturally originates from in-plane mirror symmetry breaking associated with the commensurate lock-in of the star-of-David clusters. The emergent chiral crystal structure leads to striking photon-helicity-dependent Raman peaks at different chirality. With elevating temperature to the ICDW phase, mirror symmetry is restored, realizing a chiral-to-achiral transition. Future studies can be carried out on the exotic physics of domain walls between different enantiomer domains, manipulation of the chirality [58,69], and the intricate interplay between chiral order and other rich physics (CDW, Mott insulator, QSL, superconductivity, etc.). The anomalous Raman response of the CCDW phase hints other fascinating optical

properties may exist in compounds with chiral CDW, which opens up the new revenue for new physics and device applications.

We wish to thank Dr. W. J. Shi, Dr. Y. Y. Y. Xia, and Professor G. Li for insightful discussions on tight-binding model with the Slater-Koster method; and Dr. J. Xu and Professor L. B. Gao for atomic force microscopy measurements on the samples used in the Raman study; and Dr. S. Wu and Professor S. W. Wu for optical reflectivity measurements. We acknowledge the following ARPES beamlines: BL03U and "Dreamline" of Shanghai Synchrotron Radiation Facility, and BL13U of National Synchrotron Radiation Laboratory, and BL 7.0.2 (maestro) of Advanced Light Source (this research used resources of the Advanced Light Source, a U.S. DOE Office of Science User Facility under Contract No. DE-AC02-05CH11231). We also acknowledge the Analytical Instrumentation Center of ShanghaiTech University for x-ray and Laue diffraction measurements. This work was supported by the Shanghai Municipal Science and Technology Major Project (Grant No. 2018SHZDZX02 to Y. L. C. and Z. K. L.), the National Natural Science Foundation of China (Grants No. 11634009 and No. 11674229 to Y. L. C. and Z. K. L., Grants No. 11674326, No. 11874357, and No. 12274412 to J. J. G., X. L., and Y. P. S., Grant No. 11774151 to X. X., Grant No. 12004248 to H. F. Y., and A3 Foresight Program 51861145201), the National Key R&D Program of China (Grant No. 2017YFA0305400 to Z. K. L., Grants No. 2018YFA0307000 and No. 2017YFA0303201 to X. X., and Grant No. 2021YFA1600201 to X. L. and Y. P. S.), the Joint Funds of the National Natural Science Foundation of China and the Chinese Academy of Sciences Large-Scale Scientific Facility (Grants No. U1832141, No. U1932217, and No. U2032215 to X. L. and Y. P. S.), the Key Research Program of Frontier Sciences (Grant No. QYZDB-SSW-SLH015 to J. J. G., X. L., and Y. P. S.), Excellence and Scientific Research Grant of Hefei Science Center of CAS (Grant No. 2018HSC-UE011 to J. J. G., X. L., and Y. P. S.), Shanghai Sailing Program (Grant No. 20YF1430500 to H. F. Y.). B. Y. acknowledges the financial support by the European Research Council (ERC Consolidator Grant "NonlinearTopo," No. 815869) and the MINERVA Stiftung with the funds from the BMBF of the Federal Republic of Germany.

*These authors contributed equally to this work.
†binghai.yan@weizmann.ac.il
‡yulin.chen@physics.ox.ac.uk
§xxi@nju.edu.cn
‖liuzhk@shanghaitech.edu.cn

[1] G. H. Wagnière, *On Chirality and the Universal Asymmetry Reflections on Image and Mirror Image* (Wiley-VCH, New York, 2007).
[2] W. J. Lough and I. W. Wainer, *Chirality in Natural and Applied Science* (Blackwell Science Ltd., 2002); ISBN: 978-0-632-05435-0.
[3] R. A. Hegstrom and D. K. Kondepudi, Sci. Am. **262**, 108 (1990).
[4] Y. Tokura and N. Nagaosa, Nat. Commun. **9**, 3740 (2018).
[5] R. Masuda, Y. Kaneko, Y. Tokura, and Y. Takahashi, Science **372**, 496 (2021).
[6] G. L. J. A. Rikken, J. Fölling, and P. Wyder, Phys. Rev. Lett. **87**, 236602 (2001).
[7] Y. Liu, T. Holder, and B. H. Yan, Innovation (N.Y.) **2**, 100085 (2021).
[8] P. Z. Tang, Q. Zhou, and S. C. Zhang, Phys. Rev. Lett. **119**, 206402 (2017).
[9] N. B. M. Schröter *et al.*, Nat. Phys. **15**, 759 (2019).
[10] Z. Rao *et al.*, Nature (London) **567**, 496 (2019).
[11] D. S. Sanchez *et al.*, Nature (London) **567**, 500 (2019).
[12] J. A. Wilson, F. J. Di Salvo, and S. Mahajan, Adv. Phys. **24**, 117 (1975).
[13] R. E. Thomson, B. Burk, A. Zettl, and J. Clarke, Phys. Rev. B **49**, 16899 (1994).
[14] K. Rossnagel, J. Phys. Condens. Matter **23**, 213001 (2011).
[15] K. Rossnagel and N. V. Smith, Phys. Rev. B **73**, 073106 (2006).
[16] P. Fazekas and E. Tosatti, Philos. Mag. B **39**, 229 (1979).
[17] K. T. Law and P. A. Lee, Proc. Natl. Acad. Sci. U.S.A. **114**, 6996 (2017).
[18] W. Y. He, X. Y. Xu, G. Chen, K. T. Law, and P. A. Lee, Phys. Rev. Lett. **121**, 046401 (2018).
[19] Martin Klanjšek, Andrej Zorko, Rok Žitko, Jernej Mravlje, Zvonko Jagličić, Pabitra Kumar Biswas, Peter Prelovšek, Dragan Mihailovic, and Denis Arčon, Nat. Phys. **13**, 1130 (2017).
[20] B. Sipos, A. F. Kusmartseva, A. Akrap, H. Berger, L. Forró, and E. Tutiš, Nat. Mater. **7**, 960 (2008).
[21] L. J. Li, W. J. Lu, X. D. Zhu, L. S. Ling, Z. Qu, and Y. P. Sun, Europhys. Lett. **97**, 67005 (2012).
[22] R. Ang, Y. Tanaka, E. Ieki, K. Nakayama, T. Sato, L. J. Li, W. J. Lu, Y. P. Sun, and T. Takahashi, Phys. Rev. Lett. **109**, 176403 (2012).
[23] Y. Yu *et al.*, Nat. Nanotechnol. **10**, 270 (2015).
[24] R. Ang, Z. C. Wang, C. L. Chen, J. Tang, N. Liu, Y. Liu, W. J. Lu, Y. P. Sun, T. Mori, and Y. Ikuhara, Nat. Commun. **6**, 6091 (2015).
[25] R. Ang, Y. Miyata, E. Ieki, K. Nakayama, T. Sato, Y. Liu, W. J. Lu, Y. P. Sun, and T. Takahashi, Phys. Rev. B **88**, 115145 (2013).
[26] Y. Liu, R. Ang, W. J. Lu, W. H. Song, L. J. Li, and Y. P. Sun, Appl. Phys. Lett. **102**, 192602 (2013).
[27] N. V. Smith, S. D. Kevan, and F. J. DiSalvo, J. Phys. C **18**, 3175 (1985).
[28] B. Dardel, M. Grioni, D. Malterre, P. Weibel, Y. Baer, and F. Lévy, Phys. Rev. B **46**, 7407 (1992).
[29] Th. Pillo, J. Hayoz, D. Naumović, H. Berger, L. Perfetti, L. Gavioli, A. Taleb-Ibrahimi, L. Schlapbach, and P. Aebi, Phys. Rev. B **64**, 245105 (2001).
[30] M. Arita *et al.*, Physica Amsterdam) **351B**, 265 (2004).
[31] M. Bovet, D. Popović, F. Clerc, C. Koitzsch, U. Probst, E. Bucher, H. Berger, D. Naumović, and P. Aebi, Phys. Rev. B **69**, 125117 (2004).

[32] L. Perfetti, T. A. Gloor, F. Mila, H. Berger, and M. Grioni, Phys. Rev. B **71**, 153101 (2005).
[33] K. Rossnagel, E. Rotenberg, H. Koh, N. V. Smith, and L. Kipp, Phys. Rev. Lett. **95**, 126403 (2005).
[34] F. Clerc, C. Battaglia, H. Cercellier, C. Monney, H. Berger, L. Despont, M. G. Garnier, and P. Aebi, J. Phys. Condens. Matter **19**, 355002 (2007).
[35] P. Xu, J. O. Piatek, P.-H. Lin, B. Sipos, H. Berger, L. Forró, H. M. Rønnow, and M. Grioni, Phys. Rev. B **81**, 172503 (2010).
[36] A. S. Ngankeu, S. K. Mahatha, K. Guilloy, M. Bianchi, C. E. Sanders, K. Hanff, K. Rossnagel, J. A. Miwa, C. Breth. Nielsen, M. Bremholm, and P. Hofmann, Phys. Rev. B **96**, 195147 (2017).
[37] I. Lutsyk, M. Rogala, P. Dabrowski, P. Krukowski, P. J. Kowalczyk, A. Busiakiewicz, D. A. Kowalczyk, E. Lacinska, J. Binder, N. Olszowska, M. Kopciuszynski, K. Szalowski, M. Gmitra, R. Stepniewski, M. Jalochowski, J. J. Kolodziej, A. Wysmolek, and Z. Klusek, Phys. Rev. B **98**, 195425 (2018).
[38] Y. D. Wang, W. L. Yao, Z. M. Xin, T. T. Han, Z. G. Wang, L. Chen, C. Cai, Yuan Li, and Y. Zhang, Nat. Commun. **11**, 4215 (2020).
[39] T. Ritschel, J. Trinckauf, K. Koepernik, B. Büchner, M. v. Zimmermann, H. Berger, Y. I. Joe, P. Abbamonte, and J. Geck, Nat. Phys. **11**, 328 (2015).
[40] T. Ritschel, H. Berger, and J. Geck, Phys. Rev. B **98**, 195134 (2018).
[41] M. Singh, B. Yu, J. Huber, B. Sharma, G. Ainouche, L. Fu, J. van Wezel, and M. C. Boyer, Phys. Rev. B **106**, L081407 (2022).
[42] See Supplemental Material at http://link.aps.org/supplemental/10.1103/PhysRevLett.129.156401 for methods, calculations of phonon and electronic properties, polarization- and photon-energy dependent measurements of windmill Fermi contours, detailed band structures measured with ARPES, origin for the chirality-dependent Raman response, empirical tight-binding model, chiral domain size (1 table and 34 figures), which includes Refs. [43–54].
[43] J. P. Perdew, K. Burke, and M. Ernzerhof, Phys. Rev. Lett. **77**, 3865 (1996).
[44] A. Togo and I. Tanaka, Scr. Mater. **108**, 1 (2015).
[45] G. Kresse and D. Joubert, Phys. Rev. **59**, 1758 (1999).
[46] V. Wang, N. Xu, J.-C. Liu, G. Tang, and W.-T. Geng, Comput. Phys. Commun. **267**, 108033 (2021).
[47] V. Popescu and A. Zunger, Phys. Rev. Lett. **104**, 236403 (2010).
[48] V. Popescu and A. Zunger, Phys. Rev. B **85**, 085201 (2012).
[49] W. Hayes and R. Loudon, *Scattering of Light by Crystals* (John Wiley & Sons, New York, 1978).
[50] R. Loudon, Adv. Phys. **13**, 423 (1964).
[51] I. Gregora, *Raman Scattering, International Tables for Crystallography* (2006), Vol. D, Chap. 2.3, pp. 314–328 (International Union of Crystallography).
[52] J. C. Slater and G. F. Koster, Phys. Rev. **94**, 1498 (1954).
[53] D. T. Larson, W. Chen, S. B. Torrisi, J. Coulter, S. Fang, and Efthimios Kaxiras, Phys. Rev. B **102**, 045128 (2020).
[54] X. L. Wu and C. M. Lieber, Phys. Rev. B **41**, 1239(R) (1990).
[55] R. Naaman and D. H. Waldeck, Annu. Rev. Phys. Chem. **66**, 263 (2015).
[56] B. Göhler, V. Hamelbeck, T. Z. Markus, M. Kettner, G. F. Hanne, Z. Vager, R. Naaman, and H. Zacharias, Science **331**, 894 (2011).
[57] R. Naaman, Y. Paltiel, and D. H. Waldeck, Nat. Rev. Chem. **3**, 250 (2019).
[58] A. Zong *et al.*, Sci. Adv. **4**, eaau5501 (2018).
[59] N. Shukla and A. J. Gellman, Nat. Mater. **19**, 939 (2020).
[60] S. J. Jenkins, *Chirality at Solid Surfaces* (John Wiley & Sons Ltd, New York, 2018).
[61] B. T. Fichera, A. Kogar, L. Ye, B. Gökce, A. Zong, J. G. Checkelsky, and N. Gedik, Phys. Rev. B **101**, 241106(R) (2020).
[62] Cheol-Joo Kim, A. Sánchez-Castillo, Zack Ziegler, Yui Ogawa, Cecilia Noguez, and Jiwoong Park, Nat. Nanotechnol. **11**, 520 (2016).
[63] S. Sugai, K. Murase, S. Uchida, and S. Tanaka, Physica (Amsterdam) **105B+C**, 405 (1981).
[64] O. R. Albertini, R. Zhao, R. L. McCann, S. M. Feng, M. Terrones, J. K. Freericks, J. A. Robinson, and A. Y. Liu, Phys. Rev. B **93**, 214109 (2016).
[65] S. Djurdjić Mijin *et al.*, Phys. Rev. B **103**, 245133 (2021).
[66] L. V. Gasparov, K. G. Brown, A. C. Wint, D. B. Tanner, H. Berger, G. Margaritondo, R. Gaál, and L. Forró, Phys. Rev. B **66**, 094301 (2002).
[67] E. M. Lacinska, M. Furman, J. Binder, I. Lutsyk, P. J. Kowalczyk, R. Stepniewski, and A. Wysmolek, Nano. Lett. **22**, 2385 (2022).
[68] S. Ostovar pour, L. D. Barron, S. T. Mutter, and E. W. Blanch, *Chiral Analysis: Chapter 6—Raman Optical Activity* (Elsevier, New York, 2018), pp. 249–291.
[69] S. Y. Xu *et al.*, Nature (London) **578**, 545 (2020).